https://dx.doi.org/10.1016/j.apenergy.2021.118362

This is the Pre-Published Version.

Hierarchical Distributed Multi-Energy Demand Response for Coordinated Operation of Building Clusters

Ling Zheng[a], Bin Zhou[a*], Yijia Cao[a], Siu Wing Or[b,c], Yong Li[a], Ka Wing Chan[b]

[a]*College of Electrical and Information Engineering, Hunan University, Changsha 410082, China*

[b]*Department of Electrical Engineering, The Hong Kong Polytechnic University, Hung Hom, Kowloon, Hong Kong*

[c]*Hong Kong Branch of National Rail Transit Electrification and Automation Engineering Technology Research Center, Hong Kong.*

Abstract: This paper proposes a distributed multi-energy demand response (DR) methodology for the optimal coordinated operation of smart building clusters based on a hierarchical building-aggregator interaction framework. In the proposed hierarchical framework, the aggregator acts as a digital representation of building entities to offer the multi-energy load prediction of buildings using a capsule network (CapsNet) based multi-energy demand prediction model, while these buildings leverage the load flexibility and multi-energy complementarity to implement the optimal DR for reducing individual costs. Then, a fully distributed multi-energy DR approach based on the exchange alternating direction method of multipliers (ADMM), which requires only limited information to be exchanged between the aggregator and buildings, is developed to iteratively achieve the optimal multi-energy coordination of buildings. Moreover, the proposed model can be dynamically corrected with real-time load data and weather information, and the distributed multi-energy DR approach is correspondingly optimized with rolling horizon procedures to reduce the impact of prediction uncertainties. Finally, the performance of the proposed methodology is benchmarked and validated on different scales of smart buildings, and comparative results demonstrated its superiority in solving the optimal synergistic operation problem of smart buildings.

Highlights

A hierarchical framework is proposed for multi-energy coordination of buildings

Strong couplings among multi-energy carriers are extracted using CapsNet

A digital space is formulated for model corrections with rolling horizon procedures

ADMM based distributed multi-energy DR methodology is developed

The overall energy cost can be reduced while the privacy of buildings is protected

Keywords: Integrated energy system, multi-energy coordination, distributed algorithm, capsule network, digital space.

*E-mail address of corresponding author: binzhou@hnu.edu.cn (B. Zhou).

© 2021. This manuscript version is made available under the CC-BY-NC-ND 4.0 license http://creativecommons.org/licenses/by-nc-nd/4.0/.

Nomenclature

Indices and sets

b	Index of buildings
k	Index of iteration number
t_0	Index of current time slot
t	Index of time periods
φ	Index of pollutant emissions
$\boldsymbol{x}$	Sets of decision variables

Parameters

T	The rolling horizon
N	Number of buildings
ψ	Number of pollutant emissions
c_t^e, c_t^g	Electricity price and natural gas price
β_φ^e, β_φ^g	Emissions of pollutant φ from electricity and natural gas consumption
γ^φ	Unit price of pollutant φ
P^{Lim}, V^{Lim}	Power limit of the transformer and transmission limit of natural gas
$HI_{\min}$, $HI_{\max}$	Minimum and maximum limits of HI
$M_1, M_2 \dots M_6$	Polynomial coefficients for HI
$\theta_{b,t-1}^{\mathrm{out}}$	Outdoor temperature at time t-1
$COP_{b,h}$	Coefficient of performance of appliance h
M_b, c_b, $R_{eq,b}$	Weight of air, thermal capacity of air and equivalent thermal resistance of building b
$P_{b,h,t}^{\max}$	Maximum power consumed by appliance h in building b
$\eta_b^{\mathrm{ESS,ch}}$, $\eta_b^{\mathrm{ESS,dis}}$	Charging and discharging efficiency of ESS of building b
$P_{ch,b}^{\mathrm{ESS,max}}$, $P_{dis,b}^{\mathrm{ESS,max}}$	Limits of charging and discharging power of ESS of building b
$SOC_b^{\mathrm{ESS,min}}$, $SOC_b^{\mathrm{ESS,max}}$	Minimum and maximum values of the state of charge (SOC) of ESS of building b
$E_{R,b}^{\mathrm{ESS}}$, $E_{R,b}^{\mathrm{EV}}$	Rated capacity of ESS and EV
η_b^{EV}	Charging efficiency of EV of building b
$P_b^{\mathrm{EV,max}}$	Maximum charging power of EV of building b
$SOC_b^{\mathrm{EV,min}}$, $SOC_b^{\mathrm{EV,max}}$	Minimum and maximum values of SOC of EV of building b
$SOC_b^{\mathrm{EV,out}}$	Required SOC of EV when it is leaving
T_b^a, T_b^d	Arrival time and departure time of EV
Q^{GAS}	Heating value of natural gas
η_b^{MTE}, η_b^{MTH}	Gas-electricity and gas-heat efficiencies of MT
$P_{b,\max}^{\mathrm{MTE}}$, $P_{b,\max}^{\mathrm{MTH}}$	Maximum electrical and thermal outputs of MT
η_b^{F}, $P_{b,\max}^{\mathrm{F}}$	Efficiency and maximum output of furnace
η_b^{BOH}, $P_{b,\max}^{\mathrm{BOH}}$	Efficiency and maximum output of boiler
$\varepsilon^{\mathrm{pri}}$, $\varepsilon^{\mathrm{dual}}$	Primary and dual feasibility tolerances

Variables

$P_{a,t}^{\mathrm{grid}}$, $V_{a,t}^{\mathrm{gas}}$	Electrical power and natural gas purchased by the aggregator at time slot t
$P_{b,t}$, $V_{b,t}$	Power and gas demand of building b
$HI_{b,h,t,}$, $\theta_{b,h,t}$	HI value, ambient temperature corresponding to appliance h in building b at time t
$P_{b,h,t}$	Electrical power or thermal power consumed by appliance h in building b
$P_{b,t}^{\mathrm{ESS,ch}}$, $P_{b,t}^{\mathrm{ESS,dis}}$	Charging and discharging power of ESS of building b at time t
$\varphi_{b,t}^{\mathrm{ESS,ch}}$, $\varphi_{b,t}^{\mathrm{ESS,dis}}$	Binary variables indicating charging and discharging states of ESS of building b at time t
$SOC_{b,t}^{\mathrm{ESS}}$	SOC of ESS of building b at time t
$P_{b,t}^{\mathrm{EV}}$	Charging power of EV of building b at time t
$SOC_{b,t}^{\mathrm{EV}}$	SOC of EV of building b at time t
$V_{b,t}^{\mathrm{MT}}$	Gas input of MT of building b at time t
$P_{b,t}^{\mathrm{MTE}}$, $P_{b,t}^{\mathrm{MTH}}$	Output electrical power and thermal power of MT of building b at time t
$V_{b,t}^F$, $P_{b,t}^{\mathrm{F}}$	Gas input and output thermal power of gas furnace of building b at time t
$P_{b,t}^{\mathrm{BOE}}$, $P_{b,t}^{\mathrm{BOH}}$	Input electrical power and output thermal power of boiler of building b at time t
λ_t, y_t	Dual variables associated with equilibrium constraints
u_t, α_t	
$P_{M,t}$, $V_{M,t}$	Auxiliary variables
$r_{P,t}^k$, $r_{V,t}^k$	Primal residuals and dual residuals
$s_{i,P,t}^k$, $s_{i,V,t}^k$	

1 Introduction

1.1 Motivation

Demand response (DR), benefiting from the customer flexibility, represents an effective way to reduce electrical peak loads thereby promoting the reliable and economic operation of electrical power systems [1]. In multi-energy systems (MESs), DR has been extended to multi-energy DR and breaks the barriers among different forms of energy [2]. Among the demand-side users, buildings consume a large

amount of electricity and play a significant role in DR programs [3], [4]. Nowadays, buildings are usually equipped with various energy conversion devices such as micro turbines (MTs), boilers, furnaces, as well as flexible devices such as electric vehicles (EVs), energy storage systems (ESSs), and heating/cooling systems. With the complementarity of multiple-energy carriers, smart buildings have great potential to participate in DR programs not only by adjusting the flexible loads but also by converting the source of the consumed energy [2], [5]. Therefore, the multi-energy DR of smart buildings with economic and energy-efficient advantages has become a pressing need.

Under price-based multi-energy DR programs, the electricity consumption of buildings features concentration in low electricity price periods for the sake of self-profit [6], which is prone to lead to new power peaks especially when a large number of buildings are involved [7]. In addition, during periods of high electricity prices, natural gas is consumed in large quantities to meet load demands, leading to gas consumption peaks [8]. Consequently, multi-energy DR approaches without considering the coordinated operation of buildings may cause new power and gas peaks, and further result in the overload of distribution transformers and the insufficient supply of natural gas [7], [9]. Moreover, the accurate prediction of multi-energy loads is indispensable for the investigation of advisable DR approaches. Due to the complex inherent characteristics of multi-energy loads including the strong couplings, the spatial correlations [10] and the time-varying weather factors [11], it is difficult to obtain the accurate multi-energy demand prediction for a large number of buildings. Here, this paper is devoted to investigate a distributed multi-energy DR methodology based on a hierarchical building-aggregator interaction framework to achieve the optimal coordinated operation of heterogeneous smart buildings for the overall economic efficiency enhancement.

1.2 Literature review

So far, extensive studies have been reported on multi-energy DR strategies for the optimal operation of smart buildings. In [12], the price-driven DR considering various types of appliances was formulated as a mixed-integer linear programming (MILP) model for the economic operation of smart buildings. Multi-flexibility measures were applied to promote interaction between end-users and the grid. In [13], a decision making mechanism considering multi-energy DR was proposed to facilitate effective operation of smart neighborhood. Stochastic modeling was adopted to resolve uncertainties of renewable energy sources. A multi-energy DR strategy based on the fuzzy decision making (FDM) was presented in [14] for energy management and co-optimization of smart buildings. The results demonstrated that the proposed method can reduce the purchase costs of the system as well as maintain system independence. A

genetic algorithm was developed in [15] to solve the multi-objective optimal operation problem for smart buildings considering electro-thermal DR. The relationship between the operation costs and the energy efficiency was analyzed, and the simulation results showed the economic and efficient benefits of the proposed method. Based on the market mechanism, the multi-energy DR of smart buildings was studied in [16] and [17] to achieve the coordinated clearing of electrical and thermal loads. In general, the majority of previous multi-energy DR approaches adopted centralized algorithms in which all devices of buildings were controlled and managed in a centralized manner. However, the high computation and communication overhead, and the privacy issues limit the centralized multi-energy DR approaches to solve the coordinated operation problem for a large number of smart buildings [18].

Owing to the advantages in computing scalability, communication robustness, and privacy preservation, distributed algorithms have been widely applied in DR approaches. Dantzig-Wolfe decomposition (DWD) is used in the DR scheme for peak minimization in [19], and distributed game-theoretic DR strategies were presented in [20] and [21] to improve DR efficiencies of consumers. A distributed DR approach was proposed in [22] to support the building heating demand optimization for the district heating systems, and a distributed DR algorithm was used in [23] for the electrical load management to improve the quality of DR services. However, most of previous distributed DR algorithms merely focused on loads of a single energy form. In the literature, there are a few works that optimized the multi-energy schedules of users using the distributed DR algorithms. A distributed algorithm based on the game theory was proposed in [24] to determine the optimal DR strategy for electricity-natural gas coupled networks. A distributed multi-energy DR approach was proposed in [25] for residential buildings with incomplete information. Despite achieving minimal social costs, these approaches did not consider coordinated operations among multi-energy consumers and may cause potential competitive behaviors of the consumers which are adverse to the system operation performance.

Accurate multi-energy load prediction paves the way for the investigation of multi-energy DR strategies and plays a crucial role in the optimal scheduling of MESs. Numerous state-of-art methods have been proposed to capture the coupling characteristics among multi-energy loads for enhancing the prediction accuracy. In [26], the inherent features of multi-energy load and generation were initially analyzed and then extracted by a deep belief network (DBN) based forecasting method to achieve multi-energy net load prediction. A hybrid model incorporating long-short term memory (LSTM) network, encoder-decoder and gradient boosting decision tree (GBDT) was formulated in [27] to extract temporal dynamic and coupling features of multi-energy loads to improve the prediction precision. In [28], deep multitask learning is used to capture abstract characteristics of electricity, heat, and gas loads in

industrial-park MES. In addition, an integrated Gaussian process (IGP) modeling framework in [29] and a hybrid gated recurrent unit (GRU) network in [30] were developed to cope with the spatial correlations among multi-energy loads over a certain region. Nevertheless, weather variables such as temperature, humidity, which greatly affect load variations [31], were ignored in the task of multi-energy load prediction in these studies.

1.3 Contribution

In this paper, the load flexibility and multi-energy complementarity of smart buildings are fully exploited to form a distributed multi-energy DR methodology for the optimal coordinated operation of heterogeneous buildings based on a hierarchical framework. The contributions of this paper are summarized as follows:

1. A hierarchical building-aggregator interaction framework is proposed to coordinate the optimal operation of heterogeneous smart buildings to minimize the individual energy costs and enhance DR capabilities of buildings. With the proposed hierarchical framework, the aggregator optimizes the overall purchased electricity and natural gas while buildings exploit the load flexibility and multi-energy complementarity to perform multi-energy DR, and thus the interactions between the aggregator and buildings facilitate the optimal synergies of buildings and the local multi-energy autonomy.

2. A CapsNet based multi-energy demand prediction model is formulated for the aggregator which serves as a digital representation of building entities to offer the predicted multi-energy demands. The couplings between multi-energy carriers, the weather impacts on loads, and the underlying spatial correlations among the loads from different buildings are captured by the convolution operation, and the nonlinear temporal dependencies among multi-energy load time series are further extracted by the dynamic routing mechanism between capsules.

3. A fully distributed multi-energy DR approach based on the exchange ADMM is proposed to locally determine the optimal amount of multi-energy conversion and interaction, so as to iteratively achieve the optimal coordinated operation of buildings. The proposed approach contributes to the privacy preservation since only limited information needs to be exchanged between the aggregator and buildings. Moreover, to reduce the impact of prediction uncertainties, the distributed approach is adjusted with rolling horizon procedures as the prediction model is dynamically corrected using the updated load and weather data.

2 Problem formulation

2.1 Overview of the proposed framework

Considering that competitive behaviors usually appear among different buildings under the price-based multi-energy DR programs, a hierarchical building-aggregator interaction framework is designed to coordinate the optimal operation of heterogeneous buildings. The schematic diagram of the proposed framework is illustrated in Fig. 1. The two-way communication between buildings and the aggregator is enabled through advanced metering infrastructure (AMI) including state-of-art measurement and collection systems, e.g., smart meters, and communication networks. Each building possesses any combination of the energy-consuming devices such as the EV, ESS, energy conversion devices and heating/cooling systems. Within each building, the ESS and the energy conversion devices including the MT, the gas furnace and the electric boiler are integrated in an energy hub whereby multi-energy carriers are stored, converted and conditioned [2]. The local information related to energy consumption of each building such as the appliance operation period, technical specifications of devices and energy consumption preferences could reveal the users' behaviors, habits and living pattern, etc. Thus, the users' privacy could be invaded by a third party through sniffing this detailed information. In this regard, only limited information, i.e., load profiles of buildings, weather data and the incentive signals from the aggregator, is interacted in the hierarchical framework, and the appliance-level details of buildings are maintained privacy.

In the upper level of the hierarchical framework, a CapsNet based multi-energy demand prediction model, which is driven by real-time data collected from sensors and smart meters of building entities, is formulated for the aggregator to estimate the multi-energy consumptions of building clusters and provides foundations for the optimal synergies among buildings. The collected electrical and thermal loads, the measured weather data, and the historical load data are stored in a data center, and the inherent features behind these multi-dimensional data are learned by the prediction model to simulate the multi-energy load variations in a digital space. In the lower level, buildings perform multi-energy DR to reduce their individual energy costs according to the predicted demand information and the energy price signals sent from the aggregator. In addition, the aggregator optimizes the overall electricity and natural gas purchased from the energy utility companies and determines the allocation to each building. The proposed hierarchical framework enables the real-time interactions between the aggregator and buildings thus contributing to the optimal coordinated operation of heterogeneous buildings.

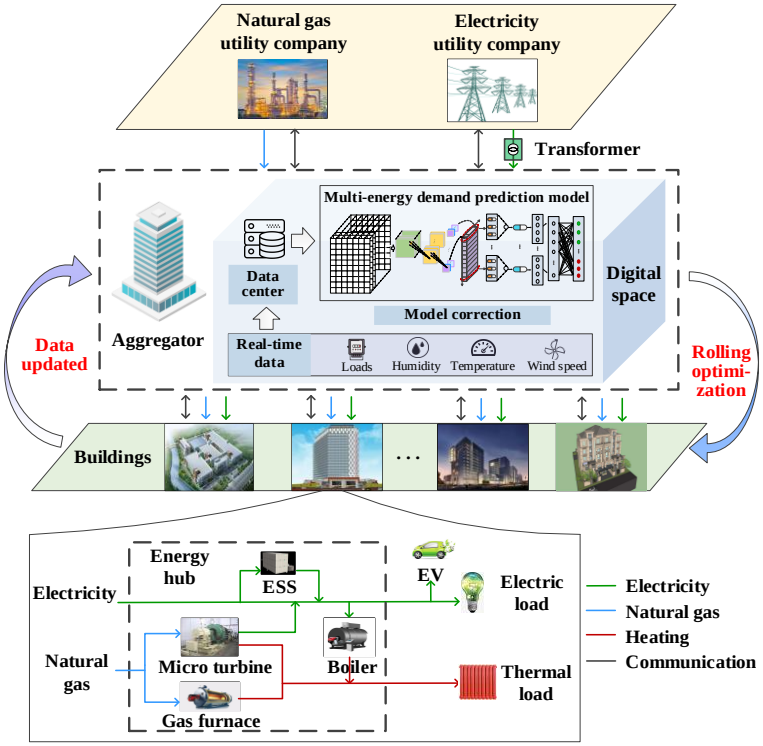

Fig. 1. Hierarchical framework for coordinated operation of heterogeneous buildings.

2.2 Multi-energy demand prediction

Multi-energy loads of a single building are strongly coupled due to the multi-energy conversion within the energy hub, and the loads of building clusters over a certain region are spatially correlated due to the similar weather conditions and socioeconomic status [29]. In addition, the load variations are closely associated with weather factors [31]. In this regard, a CapsNet based multi-energy demand prediction model capable of capturing the inherent features of the complex load and weather data is proposed to achieve simultaneous multi-energy demand predictions for building clusters. The proposed prediction model, as shown in Fig. 2, stacks a convolution sub-network with a capsule sub-network for feature extraction, and incorporates a regression layer to obtain prediction results.

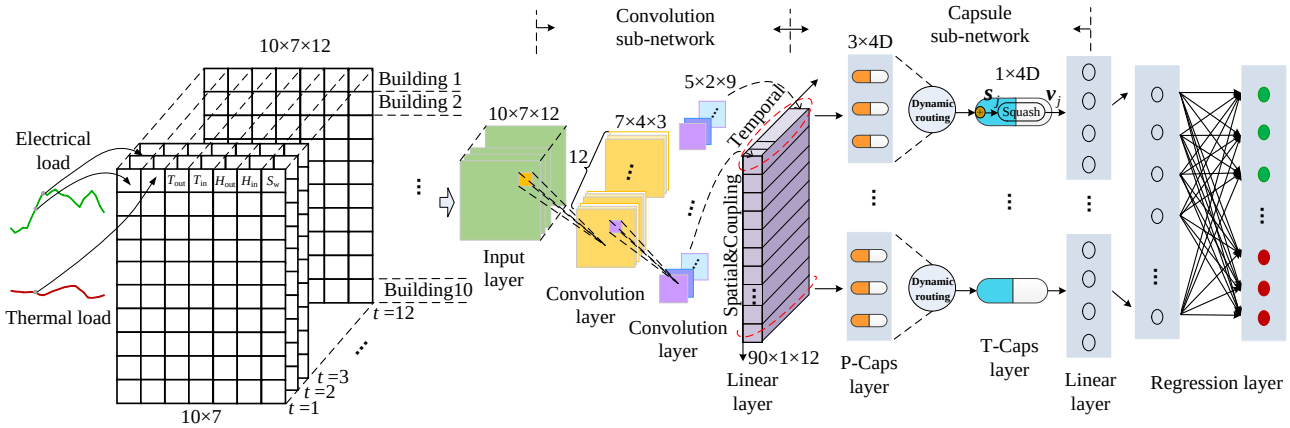

Fig. 2. CapsNet based multi-energy demand prediction model.

Firstly, the historical electrical and thermal load time series and the weather data including the internal temperature T_{in} and humidity H_{in} of buildings, as well as the external temperature T_{out}, humidity H_{out}, and wind speed S_w are represented by a 3D matrix with the size of $N \times L \times T$, where N, L and T indicate the number of buildings, the sum of the number of load types and the number of weather factors, and the length of a past time period, respectively. In this way, the historical data can be displayed as image sequences to feed into the prediction model. Then, the convolution operation with different learnable kernels, i.e., sliding windows, are performed in the first two convolution layers to learn the spatial correlations, the strong couplings, and the weather impacts. The mathematical formulation for the convolution sub-network is presented in Appendix A, Eqs.(A.1) -(A.4).

The extracted features are abstracted into network parameters and then passed through a linear layer to form as primary capsules (P-Caps). Here, a capsule is a multi-dimensional vector neuron encapsulating instantiation parameters about the features of an object [32], [33]. The length of a capsule represents the existence probability of a feature and the direction characterizes the state of the features, such as the distance between buildings, the temperature and humidity. The time capsule (T-Caps) layer is utilized to learn the temporal dependencies among the extracted spatial, coupling and weather features by the dynamic routing mechanism. The detailed calculation process of dynamic routing is shown in Appendix A, Eqs. (A.6)-(A.10). A subsequent linear layer reshapes the multi-dimensional data to 1D form and a full-connected regression layer finally outputs the predicted values of the electrical and thermal demands.

The proposed multi-energy demand prediction model is trained with historical load and weather data which are collected and updated in the data center, and thus it is considered as a data-driven model. The model parameters including the weights and bias are adjusted by the back-propagation (BP) algorithm using the updated data from the data center. The BP algorithm tries to minimize the errors between the actual load data and predicted results, and its detailed calculation is presented in Appendix A, Eqs. (A.11)-(A.15). When the algorithm converges, the accurate prediction results of multi-energy loads are obtained for further derivation of the multi-energy DR approach.

2.3 Mathematical formulation

2.3.1 Multi-energy optimization for aggregator

In this study, the aggregator is a non-profit organization whose aim is to coordinate the optimal operation of buildings with the lowest energy and environmental costs. The overall electricity and natural gas purchased from the energy utility companies are optimized by the aggregator with rolling procedures [34], and the objective function is expressed as follows,

$$\min f_a = \sum_{t=t_0}^{t_0+T} (P_{a,t}^{\text{grid}} \cdot c_t^e + V_{a,t}^{\text{gas}} \cdot c_t^g) + \sum_{\varphi=1}^{\psi} \gamma^{\varphi} (\sum_{t=t_0}^{t_0+T} (P_{a,t}^{\text{grid}} \cdot \beta_{\varphi}^e + V_{a,t}^{\text{gas}} \cdot \beta_{\varphi}^g)) \quad (1)$$

where t_0 and T denote the current time slot and the rolling horizon, respectively. At the next time step t_0+1, the new load and weather data are measured and the multi-energy demand prediction results are updated, and the optimization problem is solved using the updated information. The rolling horizon optimization procedure is repeated until the end of the optimization horizon. The aggregator maintains a balance between the energy supply and demand, and the objective (1) is subjected to the equilibrium constraints as,

$$P_{a,t}^{\text{grid}} = \sum_{b=1}^{N} P_{b,t} \quad (2)$$

$$V_{a,t}^{\text{gas}} = \sum_{b=1}^{N} V_{b,t} \quad (3)$$

In order to prevent adverse effects of power and gas peaks, which are caused by the concentrated energy consumption behaviors of buildings in response to the price signals, the aggregator coordinates the operation of buildings to ensure that the total power and natural gas purchased should not exceed the global power and gas limits, as follows,

$$P_{a,t}^{\text{grid}} \leq P^{\text{Lim}} \quad (4)$$

$$V_{a,t}^{\text{gas}} \leq V^{\text{Lim}} \quad (5)$$

2.3.2 Multi-energy demand response of buildings

The individual objectives of buildings are considered in the multi-energy DR approach such that all buildings can benefit from the flexibility and complementarity of multi-energy carriers. At the current time slot t_0, a multi-energy DR plan for the optimization horizon t_0+T is formulated based on the predictions of multi-energy demands, and buildings only perform the multi-energy DR decision for the current time. At the next rolling step t_0+1, a new multi-energy DR plan is obtained using the updated demand prediction data., such that the new multi-energy DR plan can potentially deal with uncertainties of the multi-energy demand predictions with this rolling horizon procedure [35]. The aim of buildings is to reduce their individual energy bills, and the objective function at each rolling step is expressed as,

$$\min f_b = \sum_{t=t_0}^{t_0+T} (P_{b,t} \cdot c_t^e + V_{b,t} \cdot c_t^g) \quad (6)$$

In smart buildings, not only the reducible appliances (e.g., heating/cooling systems) and the shiftable devices (e.g., EV, ESS) can provide DR capabilities, but also the inelastic/base loads can participate in DR by switching the source of the energy they consumed. Through the optimal synergistic operation of these devices, the flexibility of smart buildings can be fully made use of to enhance their DR capabilities

to reduce the energy costs. Here, the operation models of the reducible appliances, the shiftable devices and the energy conversion devices are formulated.

1) Reducible appliance modeling

The reducible appliances can be adjusted within a feasible range to maintain the users' comfort. Thermostatically controlled appliances such as heating/cooling systems are the main reducible appliances [36], [37] in smart buildings and can participant in DR by changing the temperature settings. The Heat Index (HI), which combines temperature and relative humidity, is a comfort index to indicate human-perceived equivalent temperature [38]. This metric can be used to measure the thermal comfort violation level due to the adjustment of heating/cooling systems. The calculation formula is expressed as follows,

$$\begin{aligned} HI_{b,h,t} = {} & M_1 \cdot \theta_{b,h,t} + M_2 \cdot \theta_{b,h,t} \cdot R_t + M_3 \cdot (\theta_{b,h,t})^2 + M_4 \cdot (\theta_{b,h,t})^2 \cdot R_t \\ & + M_5 \cdot \theta_{b,h,t} \cdot (R_t)^2 + M_6 \cdot (\theta_{b,h,t})^2 \cdot (R_t)^2 + F_R(R_t) \end{aligned} \tag{7}$$

where R_t represents the relative humidity, and $F_R(\cdot)$ is the polynomial function with respect to R_t. Eq. (8) imposes the limits on HI,

$$HI_{\min} \le HI_{b,h,t} \le HI_{\max} \tag{8}$$

The indoor ambient temperature of buildings depends on the materials used in the walls, glasses, the structure of buildings and the outdoor temperature, etc. In this study, the relationship between the indoor temperature and the energy consumed by heating/cooling systems is represented by the equivalent thermal resistance temperature model in [39], as follows,

$$\begin{aligned} \theta_{b,h,t} = {} & (1 - \frac{\Delta t}{1000 \cdot M_b \cdot c_b \cdot R_{\mathrm{eq},b}}) \cdot \theta_{b,h,t-1} + \frac{\Delta t}{1000 \cdot M_b \cdot c_b \cdot R_{\mathrm{eq},b}} \cdot \theta_{b,t-1}^{\mathrm{out}} \\ & + \frac{COP_{b,h} \cdot P_{b,h,t} \cdot \Delta t}{0.000277 \cdot M_b \cdot c_b}, \forall t > 1 \end{aligned} \tag{9}$$

$$0 \le P_{b,h,t} \le P_{b,h,t}^{\max} \tag{10}$$

where $P_{b,h,t}$ represents the electrical power consumed by the appliance if it is supplied by electricity, or represents the consumed thermal power if it is supplied by thermal energy. Note that if the heating/cooling system is operated for heating, the sign in the second term in Eq. (9) is a plus, while if it is operated for cooling, the sign needs to be changed to a minus.

2) Shiftable device modeling

The shiftable devices can be shifted to different time slots in a certain optimization horizon, and the total energy consumed remains fixed. The ESS and EV, as two typical shiftable devices, are modeled in this study. The operation constraints of the ESS are introduced as,

$$SOC_{b,t}^{\mathrm{ESS}} = SOC_{b,t-1}^{\mathrm{ESS}} + \left(\frac{\eta_b^{\mathrm{ESS,ch}} \cdot P_{b,t}^{\mathrm{ESS,ch}}}{E_{\mathrm{R},b}^{\mathrm{ESS}}} - \frac{P_{b,t}^{\mathrm{ESS,dis}}}{\eta_b^{\mathrm{ESS,dis}} \cdot E_{\mathrm{R},b}^{\mathrm{ESS}}}\right) \cdot \Delta t \tag{11}$$

$$SOC_b^{\mathrm{ESS,min}} \le SOC_{b,t}^{\mathrm{ESS}} \le SOC_b^{\mathrm{ESS,max}} \tag{12}$$

$$0 \le P_{b,t}^{\mathrm{ESS,ch}} \le P_{\mathrm{ch},b}^{\mathrm{ESS,max}} \varphi_{b,t}^{\mathrm{ESS,ch}} \tag{13}$$

$$0 \le P_{b,t}^{\mathrm{ESS,dis}} \le P_{\mathrm{dis},b}^{\mathrm{ESS,max}} \varphi_{b,t}^{\mathrm{ESS,dis}} \tag{14}$$

$$\varphi_{b,t}^{\mathrm{ESS,ch}} + \varphi_{b,t}^{\mathrm{ESS,dis}} \le 1 \tag{15}$$

Eq. (13) and Eq. (14) impose the limits on the charging and discharging power, respectively.

The modeling of the EV is similar to that of the ESS and the operation constraints of the EV for each building can be expressed as follows,

$$SOC_{b,t}^{\mathrm{EV}} = SOC_{b,t-1}^{\mathrm{EV}} + \eta_b^{\mathrm{EV}} \cdot \frac{P_{b,t}^{\mathrm{EV}}}{E_{\mathrm{R},b}^{\mathrm{EV}}} \cdot \Delta t,\ t \in [T_b^a, T_b^d] \tag{16}$$

$$0 \le P_{b,t}^{\mathrm{EV}} \le P_b^{\mathrm{EV,max}},\ t \in [T_b^a, T_b^d] \tag{17}$$

$$SOC_b^{\mathrm{EV,min}} \le SOC_{b,t}^{\mathrm{EV}} \le SOC_b^{\mathrm{EV,max}},\ t \in [T_b^a, T_b^d] \tag{18}$$

$$SOC_{b,t}^{\mathrm{EV}} \ge SOC_b^{\mathrm{EV,out}},\ t = T_b^d \tag{19}$$

Eq. (17) and Eq. (18) impose the limits on the charging power and the SOC of the EV, respecively. Note that the EV should be charged with the required state of energy before leaving, as described in Eq. (19), where $SOC_b^{\mathrm{EV,out}}$ represents the required SOC of the EV when it is leaving.

3) Energy conversion device modeling

The energy conversion devices in this study incorporate the MT, the gas furnace and the electric boiler. The operation constraints of the energy conversion devices are formulated as Eqs. (20)-(27).

$$P_{b,t}^{\mathrm{MTE}} = V_{b,t}^{\mathrm{MT}} \cdot \eta_b^{\mathrm{MTE}} \cdot Q^{\mathrm{GAS}} \tag{20}$$

$$P_{b,t}^{\mathrm{MTH}} = V_{b,t}^{\mathrm{MT}} \cdot \eta_b^{\mathrm{MTH}} \cdot Q^{\mathrm{GAS}} \tag{21}$$

$$0 \le P_{b,t}^{\mathrm{MTE}} \le P_{b,\max}^{\mathrm{MTE}} \tag{22}$$

$$0 \le P_{b,t}^{\mathrm{MTH}} \le P_{b,\max}^{\mathrm{MTH}} \tag{23}$$

$$P_{b,t}^{\mathrm{F}} = V_{b,t}^{\mathrm{F}} \cdot \eta_b^{\mathrm{F}} \cdot Q^{\mathrm{GAS}} \tag{24}$$

$$0 \le P_{b,t}^{\mathrm{F}} \le P_{b,\max}^{\mathrm{F}} \tag{25}$$

$$P_{b,t}^{\mathrm{BOH}} = P_{b,t}^{\mathrm{BOE}} \cdot \eta_b^{\mathrm{BOH}} \tag{26}$$

$$0 \le P_{b,t}^{\mathrm{BOH}} \le P_{b,\max}^{\mathrm{BOH}} \tag{27}$$

4) Multi-energy coupling constraint

As depicted in Fig.1, the energy conversion devices and the ESS are integrated in an energy hub such that the electricity, natural gas and heat are coupled. In order to model the multi-energy couplings and the interior topology, a multi-energy coupling matrix $\boldsymbol{C}_b$ is formulated, as follows,

$$\underbrace{\begin{bmatrix} L_{b,t}^{\mathrm{e}} \\ L_{b,t}^{\mathrm{h}} \end{bmatrix}}_{\boldsymbol{L}_b} = \underbrace{\begin{bmatrix} \nu_{e,P} & Q^{\mathrm{GAS}}\nu_{\mathrm{MT}}\eta_b^{\mathrm{MTE}}\nu_{e,V} & \nu_{e,E} \\ \nu_{\mathrm{B}}\eta_b^{\mathrm{BOH}}\nu_{h,P} & Q^{\mathrm{GAS}}(\nu_{\mathrm{MT}}\eta_b^{\mathrm{MTE}}\nu_{\mathrm{B}}\eta_b^{\mathrm{BOH}} + \nu_{\mathrm{MT}}\eta_b^{\mathrm{MTH}} + \nu_{\mathrm{F}}\eta_b^{\mathrm{F}})\nu_{h,V} & \nu_{\mathrm{B}}\eta_b^{\mathrm{BOH}}\nu_{h,E} \end{bmatrix}}_{\boldsymbol{C}_b} \underbrace{\begin{bmatrix} P_{b,t} \\ V_{b,t} \\ P_{b,t}^{\mathrm{ESS}} \end{bmatrix}}_{\boldsymbol{E}_b} \tag{28}$$

where $\boldsymbol{E}_b$ and $\boldsymbol{L}_b$ represent the input vector and output vector of the energy hub in building b, respectively; $\nu_{e,P}$, $\nu_{e,V}$, $\nu_{e,E}$, are dispatch factors of the input energy resources to the electrical loads; $\nu_{h,P}$, $\nu_{h,V}$, $\nu_{e,E}$ are dispatch factors of the input energy resources to the thermal loads; ν_{MT}, ν_{B}, ν_{F} are dispatch factors of the input energy resources to the MT, electric boiler and furnace, respectively. Note that both the base loads and the elastic loads are included in the output load vector $\boldsymbol{L}_b$. In order to avert the nonlinearity introduced by dispatch factors, a state variable-based method in [40] is used to designate the outputs of the energy conversion devices $P_{b,t}^{\mathrm{BOH}}$, $P_{b,t}^{\mathrm{F}}$ and $P_{b,t}^{\mathrm{MTE}}$ as state variables. Without introducing the dispatch factors, the multi-energy coupling matrix can be reformulated as Eq. (29), where $\boldsymbol{C}_b'$ and $\boldsymbol{E}_b'$ are the linear coupling matrix and the extended input energy vector, respectively.

$$\underbrace{\begin{bmatrix} L_{b,t}^{\mathrm{e}} \\ L_{b,t}^{\mathrm{h}} \\ 0 \end{bmatrix}}_{\boldsymbol{L}_b} = \underbrace{\begin{bmatrix} 1 & -1/\eta_b^{\mathrm{BOH}} & 0 & 1 & 0 & 1 \\ 0 & 1 & 1 & \eta_b^{\mathrm{MTH}}/\eta_b^{\mathrm{MTE}} & 0 & 0 \\ 0 & 0 & -1/Q^{\mathrm{GAS}}\eta_b^{\mathrm{F}} & -1/Q^{\mathrm{GAS}}\eta_b^{\mathrm{MTE}} & 1 & 0 \end{bmatrix}}_{\boldsymbol{C}_b'} \underbrace{\begin{bmatrix} P_{b,t} \\ P_{b,t}^{\mathrm{BOH}} \\ P_{b,t}^{\mathrm{F}} \\ P_{b,t}^{\mathrm{MTE}} \\ V_{b,t} \\ P_{b,t}^{\mathrm{ESS}} \end{bmatrix}}_{\boldsymbol{E}_b'} \tag{29}$$

3 Distributed multi-energy DR approach

The computational complexity of the multi-energy optimization problem Eq. (1)-Eq. (27) and Eq. (29) increases significantly as the number of buildings grows. Also, the detailed information related to the technical parameters of devices and the energy usage preferences of users are not willing to be shared. Therefore, a fully decentralized ADMM based multi-energy DR approach is developed to decompose the original optimization problem into independent decision-making sub-problems to achieve the local multi-energy autonomy for buildings. Appendix B explains how the problem is solved with an iterative process.

The information interaction between the aggregator and buildings is depicted in Fig. 3. At time slot t_0,

buildings locally solve the optimization sub-problem by the distributed multi-energy DR approach based on the predicted demand information $\hat{\boldsymbol{L}}_{i,t_0}$ from the aggregator. Specifically, in each iteration of the distributed multi-energy DR approach, the aggregator and buildings independently solve their local sub-problem in a parallel manner and the power and natural gas demand of each participant, i.e., $P_{i.t}^k$ and $V_{i.t}^k$, are updated. The average power and gas of all participants are given by $\bar{P}_t^k = (1/M)\sum_{i=1}^M P_{i.t}^k$ and $\bar{V}_t^k = (1/M)\sum_{i=1}^M V_{i.t}^k$, which can be regarded as unbalanced power and gas between the aggregator and the buildings, and $P_{i.t}^k - \bar{P}_t^k$ and $V_{i.t}^k - \bar{V}_t^k$ are the contributions that every participant needs to provide, as presented in Eq. (B.8). Then, the dual variables u_t and α_t, which can be regarded as incentive signals corresponding to the electricity and natural gas prices, are updated according to the average power and natural gas of all participants, as shown in Appendix B, Eqs. (B.13)-(B.14). For the next iteration, the aggregator sends the updated incentive signals to the buildings, and the buildings solve their individual multi-energy DR problem and then send back their solution to the aggregator. The iterative optimization process drives $\bar{P}_t^k$ and $\bar{V}_t^k$ to move towards zero, and the distributed algorithm finally converges to the optimal solution. As the unbalanced energies are evenly shared by all participants during the iterative process, this distributed algorithm fairly resolve competition behaviors of buildings. When the buildings have implemented the current DR strategy, the new load and weather data $\boldsymbol{y}_{i,t_0}$ are measured and stored in the data center of the aggregator for the optimization in next time t_0+1.

The detailed implementation steps for the proposed hierarchical distributed multi-energy DR methodology are illustrated in Fig. 4. It can be seen that only a little information, i.e., the incentive signals from the aggregator and the demand and weather information from buildings, needs to be exchanged to achieve the optimal multi-energy coordination of heterogeneous buildings in the proposed methodology. Thus, the communication burden is significantly lightened making the distributed multi-energy DR approach much scalable, and meanwhile the detailed multi-energy management within each building are kept confidential.

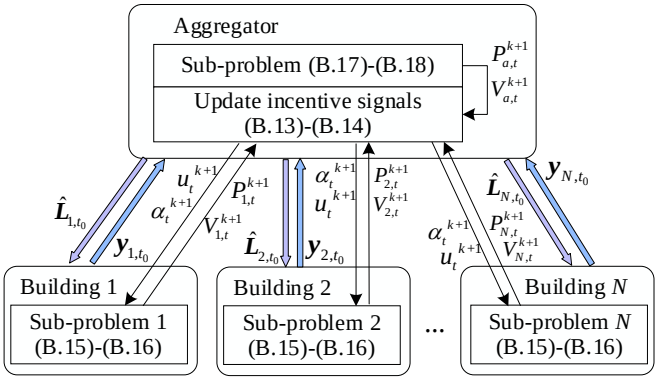

Fig. 3. Information interaction between the aggregator and buildings.

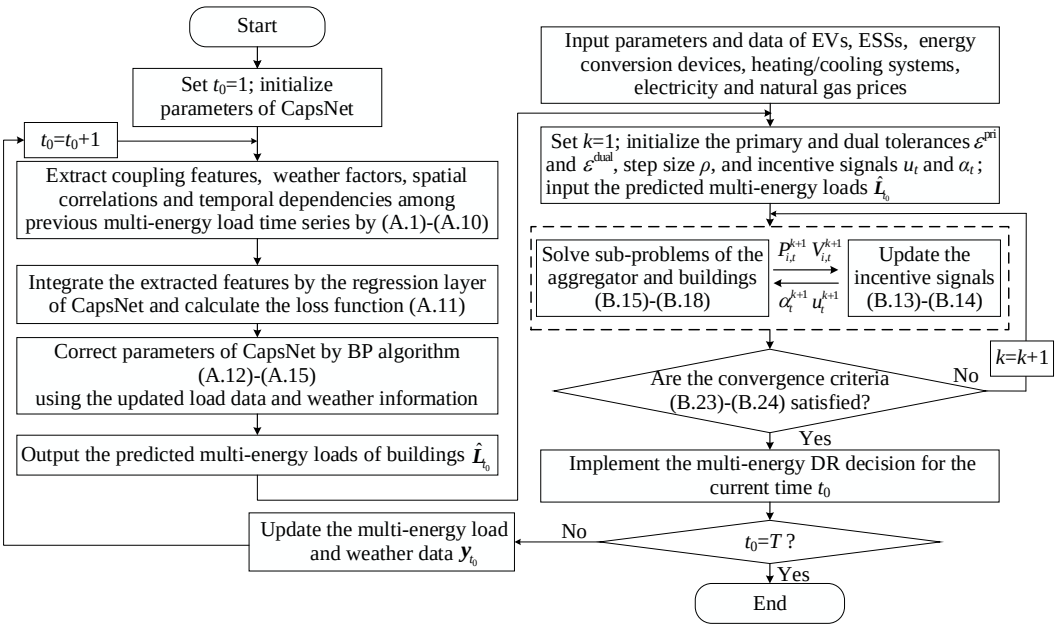

Fig. 4. Implementation framework of the proposed methodology.

4 Case studies

4.1 System data and load prediction

The proposed hierarchical distributed multi-energy DR methodology is studied on a typical MES in Northern China. The MES is comprised of 10 heterogeneous smart buildings with different load behaviors and supplied by a 1250kVA three-phase transformer. The Time-of-Use (ToU) tariff electricity price is illustrated in Fig. 5 and the natural gas price is set as 0.56 \$/m^3. The technical specifications of the ESSs, EVs and energy conversion devices of the buildings are listed in Table 1-3. The pollutant emission parameters of the electricity and natural gas consumption, as well as the environmental cost factors are given in Table 4, which are derived from [41], [42].

Table 1 Technical specifications of ESSs.

ESS	$P_{\mathrm{ch},b}^{\mathrm{ESS,max}} = P_{\mathrm{dis},b}^{\mathrm{ESS,max}}$=[30, 20, 40, 60, 30, 25, 30, 20, 30,50] kW	$\eta_b^{\mathrm{ESS,ch}} = \eta_b^{\mathrm{ESS,dis}}$ =[0.9, 0.9, 0.9, 0.9, 0.9, 0.9, 0.9, 0.9, 0.9, 0.9]
	$SOC_b^{\mathrm{ESS,min}}$=[0.4, 0.4, 0.4, 0.4, 0.4, 0.4, 0.4, 0.4, 0.4, 0.4]	$SOC_b^{\mathrm{ESS,max}}$=[0.9, 0.9, 0.9, 0.9, 0.9, 0.9, 0.9, 0.9, 0.9, 0.9]
	$E_{\mathrm{R},b}^{\mathrm{ESS}}$=[150, 120, 200, 180, 160, 100, 150, 80,130, 160] kWh	

Table 2 Technical specifications of EVs.

EV	$P_b^{\mathrm{EV,max}}$=[20, 25, 15, 30, 25, 25, 40, 25, 30, 35] kW	η_b^{EV} =[0.9, 0.9, 0.9, 0.9, 0.9, 0.9, 0.9, 0.9, 0.9, 0.9]
	$SOC_b^{\mathrm{EV,min}}$=[0.4, 0.4, 0.4, 0.4, 0.4, 0.4, 0.4, 0.4, 0.4, 0.4]	$SOC_b^{\mathrm{EV,max}}$=[0.9, 0.9, 0.9, 0.9, 0.9, 0.9, 0.9, 0.9, 0.9, 0.9]

	$SOC_b^{\mathrm{EV,end}}$=[0.85, 0.8, 0.7, 0.75, 0.7, 0.85, 0.8, 0.65, 0.75, 0.9]	$E_{\mathrm{R},b}^{\mathrm{EV}}$=[100, 120, 80, 100, 125, 100, 150, 140, 120, 130] kWh

Table 3 Technical specifications of energy conversion devices.

MT	η_b^{MTE} =[0.45, 0.45, 0.45, 0.45, 0.45, 0.45, 0.45, 0.45, 0.45, 0.45]	η_b^{MTH} =[0.4, 0.4, 0.4, 0.4, 0.4, 0.4, 0.4, 0.4, 0.4, 0.4]
	$P_{b,\max}^{\mathrm{MTE}}$=[60, 65, 50, 65, 80, 70, 75, 50, 65, 80] kW	
Furnace	$P_{b,\max}^{\mathrm{F}}$=[25, 20, 30, 20, 25, 30, 25, 25, 30, 25] kW	η_b^{F} =[0.8, 0.8, 0.8, 0.8, 0.8, 0.8, 0.8, 0.8, 0.8, 0.8]
Boiler	$P_{b,\max}^{\mathrm{BOH}}$=[40, 35, 30, 35, 45, 50, 35, 40, 45, 40] kW	η_b^{BOH}=[0.75, 0.75, 0.75, 0.75, 0.75, 0.75, 0.75, 0.75, 0.75, 0.75]

Table 4 Pollutant emission parameters and environmental cost factors.

Pollutants	CO_2	SO_2	NO_x
Electricity (kg/kWh)	0.92	0.0005	0.002
Natural gas (kg/10^6m^3)	2.01	11.6	0.0062
Environmental value ($/kg)	0.004	0.93	1.24

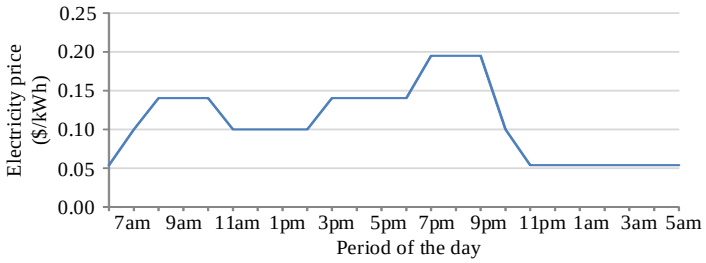

Fig.5. Time-of-Use (ToU) tariff electricity price.

To validate the effectiveness of the CapsNet based multi-energy demand prediction method, the load and weather data in December in 2019 are used for simulation and the sampling interval is 1h. To intuitively illustrate the multi-energy load prediction results of different methods, building 5 is selected as an example of these buildings and the prediction results on the 26th are shown in Fig. 6. It can be seen that the prediction results of the proposed prediction model show more similar contours and variation trends to the real multi-energy load data than the results of other methods. Thus, the proposed model is suitable for multi-energy demand of buildings. The daily electrical and thermal load profiles of buildings on the same day of the next month predicted by the CapsNet based prediction model are depicted in Fig. 7. In this study, the electrical and thermal base loads account for 70% and 40% of the total electrical and thermal demands respectively. The heating/cooling system is supplied by thermal energy and the maximum power consumption $P_{b,h,t}^{\max}$ shall not exceed 60% of the total thermal demands. The parameters related to the equivalent thermal resistance temperature model of buildings are adapted from [36]. The comfort indoor temperature is assumed to be distributed between [20℃, 25℃]. The initial SOC and the

arrival/departure time of the EVs are gathered from [43], [44]. The maximum natural gas limit is set as 80 m^3 [8]. With regard to the ADMM algorithm, the penalty parameter ρ is set as 2, and the primary feasibility tolerance ε^{pri} and the dual feasibility tolerance $\varepsilon^{\text{dual}}$ are set as 0.1 and 1 respectively [45]. The multi-energy DR methodology is performed over one day with 24-time slots, and all the tests are implemented in Matlab R2018b with YALMIP toolbox and solved by CPLEX solver on a 64-bit personal computer.

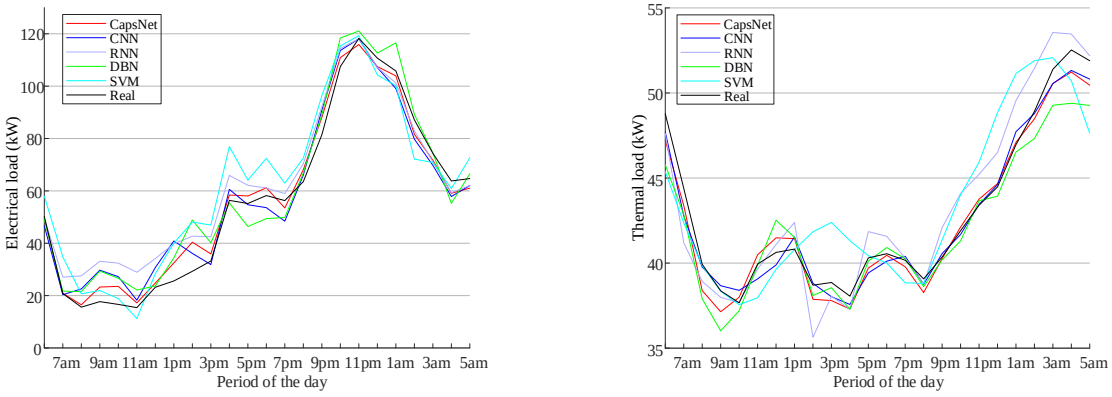

(a) (b)

Fig. 6. Load prediction results of building 5 by different prediction methods (a) predicted electrical load profiles, (b) predicted thermal load profiles.

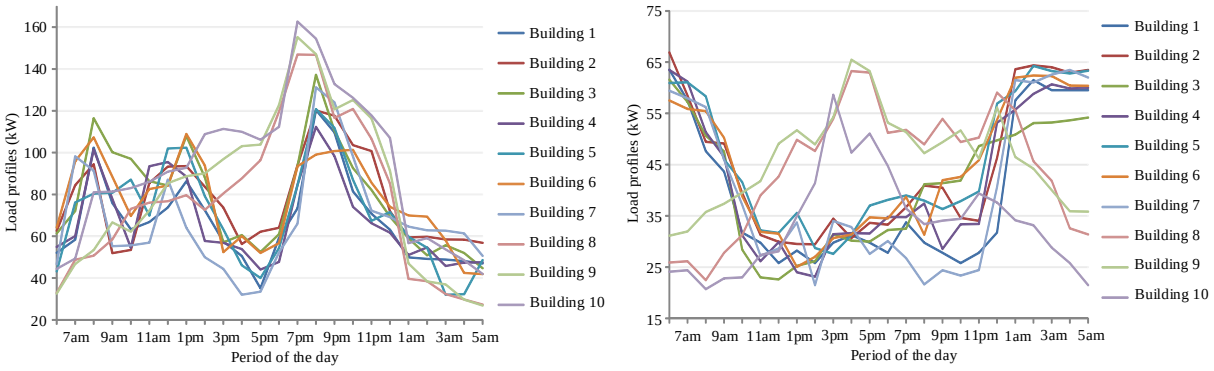

(a) (b)

Fig. 7. Load prediction results of 10 buildings by CapsNet (a) predicted electrical load profiles, (b) predicted thermal load profiles.

4.2 Comparative results and analysis

To verify the effectiveness of the proposed multi-energy DR methodology, three schemes are performed for comparison: 1) Scheme 1 is the conventional electricity and natural gas scheduling without the implementation of multi-energy DR. The dispatch factors are set as 0.5, 0.3 and 0.2 for the MT, furnace and boiler, respectively; 2) Scheme 2 performs centralized multi-energy DR in previous studies [13] without considering the optimal coordinated operation of buildings; 3) Scheme 3 employs the proposed distributed multi-energy DR methodology.

Fig. 8 depicts the total electrical power purchased from the electricity utility company with the schemes 1-3. As can been seen from the figures, without the implementation of multi-energy DR, the input power of scheme 1 reaches the peak during the period of high electricity price, i.e., 7pm to 9pm. In contrast, the power consumption during 7pm to 9pm is considerably reduced by using the centralized multi-energy DR scheme 2, but more severe new power peaks appear during the periods of low electricity prices, i.e., from 11pm to 6am. This is because, without considering the optimal coordinated operations among buildings, the power consumed by the buildings is concentrated during the period of the lowest electricity price, thus violating the power limit of the transformer. Compared with schemes 1 and 2, the electrical power peaks are flattened due to the optimal synergies of buildings with the proposed distributed multi-energy DR methodology. Fig. 9 shows the total natural gas purchased from the natural gas utility company. It can be observed that natural gas is heavily consumed with scheme 1 to meet the large thermal demands at night and early morning. As the energy source can be switched from natural gas to electricity based on the thermal demands with schemes 2-3, the natural gas input is significantly reduced during 11pm-7am. However, the natural gas purchased in scheme 2 exceeds the transmission limit of natural gas from 7am to 9am. The electricity price in this period is higher than that in previous time, and thus natural gas is preferentially consumed. It can be summarized from Figs.8-9 that the power and natural gas peaks can be effectively shaved with the proposed distributed multi-energy DR methodology as the optimal multi-energy coordination of smart buildings is achieved.

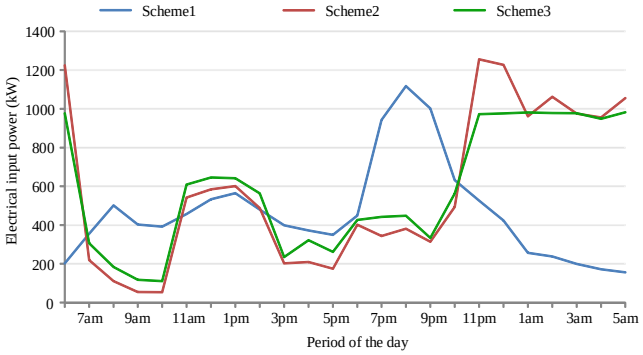

Fig. 8. Total purchased electrical power from the electricity utility with scheme 1-3.

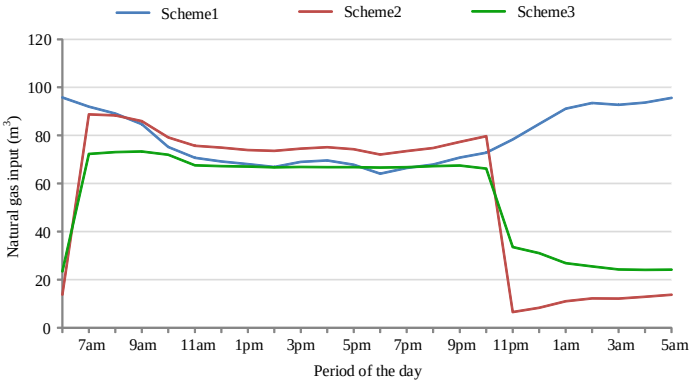

Fig. 9. Total purchased natural gas from the natural gas utility with scheme 1-3.

The comparative economic performance results of buildings on energy costs with schemes 1-3 are presented in Table 5. It can be seen that both the electricity cost and the natural gas cost for each building with scheme 1 are the highest. With the implementation of multi-energy DR, the energy costs with scheme 2 and scheme 3 are substantially reduced. As one energy resource with lower price cannot be substituted indefinitely by another resource with higher price to avoid new energy consumption peaks in scheme 3, the energy costs of scheme 3 for each building are higher than those of scheme 2. Table 6 presents the comparative results of schemes 1-3 on the energy cost, environmental cost and total cost of the aggregator. In contrast with scheme 1, the energy cost and environmental cost of scheme 2 are reduced by 24.10% and 8.18%, respectively, while those of scheme 3 are decreased by 21.04% and 5.68%, respectively. It can be concluded that multi-energy synergies can be made use of by scheme 2 and scheme 3 to fulfill the demands with lower energy and environmental costs. Although obtaining satisfying economic performance, scheme 2 cannot guarantee the secure and reliable operation of the system as competitive behaviors appear among the buildings without the optimal coordinated operation. The proposed distributed multi-energy DR methodology can reduce the economic costs and meanwhile shave electrical power and gas peaks to enhance the operation performance of the whole MES.

Table 5 Comparative economic performance results of buildings with scheme 1-3.

Index of buildings	Scheme1			Scheme2			Scheme3		
	Electricity cost ($)	Natural gas cost ($)	Energy cost ($)	Electricity cost ($)	Natural gas cost ($)	Energy cost ($)	Electricity cost ($)	Natural gas cost ($)	Energy cost ($)
1	119.73	103.44	223.17	98.48	69.53	168.01	107.32	68.13	175.44
2	138.33	107.97	246.30	113.64	78.24	191.88	118.33	80.18	198.52
3	140.98	104.94	245.92	121.47	71.96	193.43	128.13	72.49	200.62
4	125.16	105.52	230.68	89.16	76.15	165.31	95.12	77.24	172.36
5	128.64	108.85	237.49	89.99	80.90	170.90	102.22	77.04	179.26
6	136.77	107.93	244.70	115.99	71.57	187.56	125.72	69.67	195.38
7	129.26	104.10	233.35	81.47	81.14	162.61	93.94	77.44	171.38
8	149.49	107.87	257.35	145.17	68.36	213.52	152.83	67.35	220.17
9	162.00	109.49	271.49	139.35	73.54	212.89	148.77	71.45	220.22
10	188.44	98.21	286.65	139.62	74.41	214.03	151.81	70.70	222.51

Table 6 Comparative cost results of the aggregator with scheme 1-3.

Scheme	1	2	3
Energy cost ($)	2477.11	1880.13	1955.85
Environmental cost ($)	94.11	86.41	88.76
Total cost ($)	2571.22	1966.54	2044.61

Fig. 10 shows the charging power of EVs for each building with scheme 2 and scheme 3. It can be observed that the EVs in scheme 2 are mainly charged during hours with the lowest electricity price, i.e., 11pm-5am, while the charging durations of EVs in scheme 3 are different as the leaving time, arriving time and technical specifications are varied. Besides, the charging power of EVs in scheme 2 is larger than that in scheme 3, which is likely to cause power peaks during the period of low electricity price. Due to the optimal coordinated operation of buildings, the charging time of EVs in scheme 3 is dispersed to various periods after their arrival, rather than concentrated in the period with the lowest electricity price. Fig. 11 shows the charging/discharging power of ESSs with schemes 2-3. It can be found that the charging/discharging periods of ESSs in scheme 2 are similar with those in scheme 3. Compared with scheme 2, the charging power of ESSs in scheme 3 is lower during the periods of low electricity prices. Correspondingly, the discharging power of ESSs in scheme 3 is lower during high-price periods, thus causing more electricity expenses.

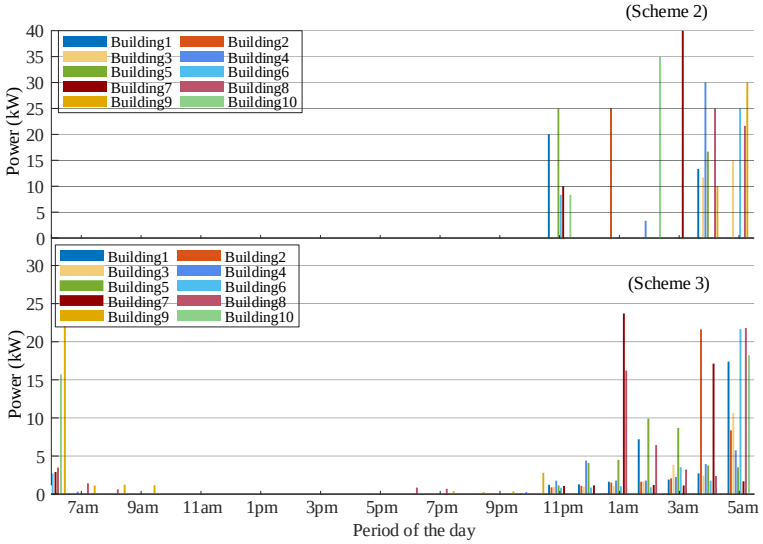

Fig. 10. Charging power of EVs with schemes 2-3.

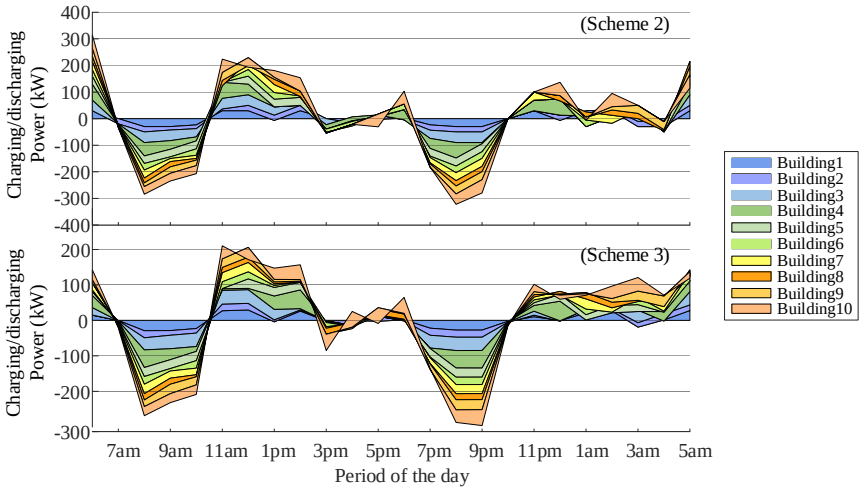

Fig. 11. Charging/discharging power of ESSs with schemes 2-3.

Figs. 12 and 13 illustrate the electrical and thermal outputs of MTs for each building with schemes 2-3, respectively, and Figs. 14-15 depict the output curves of the boilers and the furnaces. It is observed in scheme 2 that the MTs only work during 6am-11pm when electricity prices are relatively high to produce electricity and heat, while the boilers only operate during the hours 10pm-7am with low electricity prices. Since the thermal loads are mainly supplied by electric boilers at night and early morning, power peaks could occur during these periods. In addition, the furnaces serve as a supplement to fulfill the thermal demands throughout the day, and their outputs are adjusted to follow the thermal load profiles. In contrast, the MTs, boilers and furnaces are jointly optimized all the day to fulfill the demands of buildings in scheme 3. Furthermore, the outputs of furnaces in scheme 3 are larger than those of scheme 2, while the thermal outputs of boilers and MTs in scheme 3 are smaller compared with those of scheme 2. Thus the furnaces are prioritized to supply the thermal demands in scheme 3 due to their high energy conversion efficiency.

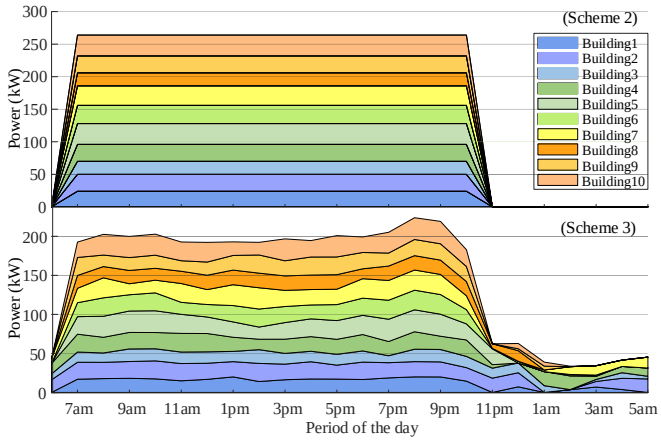

Fig. 12. The curves of electrical outputs of MTs.

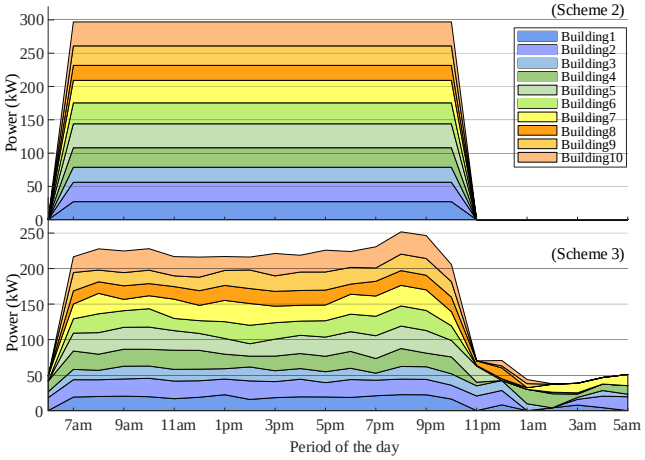

Fig. 13. The curves of thermal outputs of MTs.

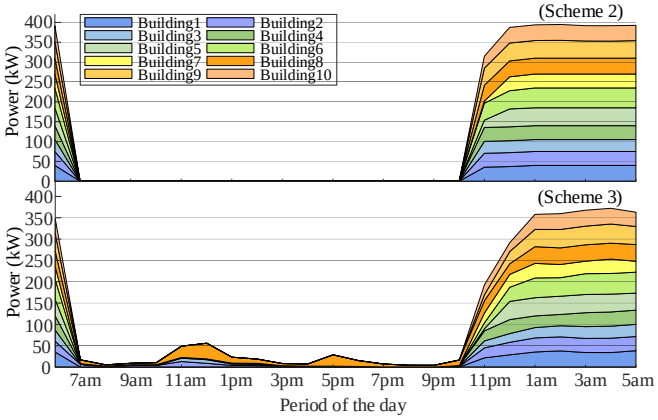

Fig. 14. The output curves of boilers.

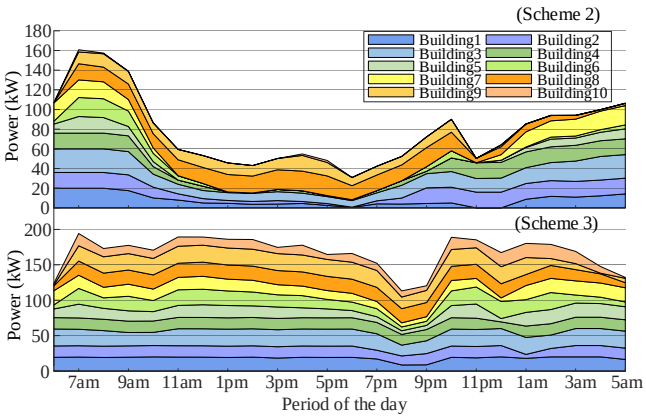

Fig. 15. The output curves of furnaces.

The heterogeneous buildings possess various devices with technical specifications that are not necessarily the same, and thus the response characteristics of each building are varied. The daily energy analytics of various devices for two representative buildings, a residential building (building 2) and a

commercial building (building 9), in scheme 3 are shown in Figs. 16-17. It can be observed that the EV in building is mainly charged during the night, while the charging time for the EV in building 9 is more flexible and mainly in the daytime. Besides, the power of the furnace and the heating system in building 9 drops at night, while the power of the heating system increases and the power of the furnace is almost invariant late at night. This is because residents are at home at night and residential buildings have higher electricity and heat demands than during the day. Moreover, the power of the boiler grows while the power of the MT decreases in both buildings, which is resulting from the low electricity price at night.

It can be concluded from the comparative studies that the flexibility provided by EVs, ESSs and multi-energy conversion devices is fully exploited by the proposed distributed multi-energy DR methodology to fulfill the multi-energy demands of buildings with reduced individual costs. Meanwhile, the power peaks and natural gas peaks are shaved through the optimal multi-energy coordination of heterogeneous smart buildings thus facilitating the secure and reliable operation for the MES.

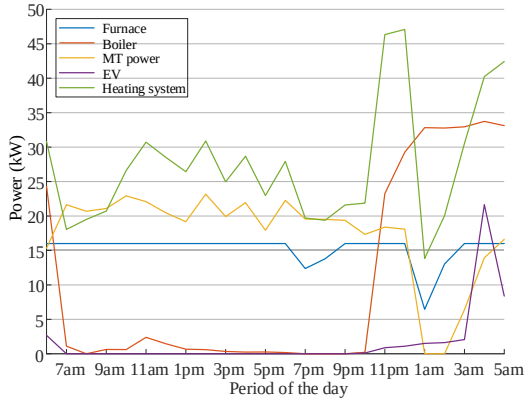

Fig. 16. Energy analytics of various devices for building 2.

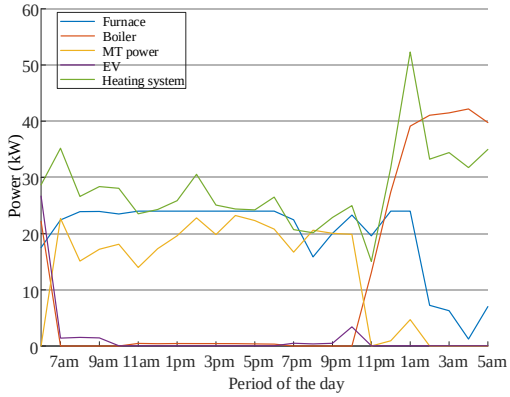

Fig. 17. Energy analytics of various devices for building 9.

4.3 Discussion

4.3.1 Convergence and scalability

In order to verify the convergence of the proposed distributed multi-energy DR methodology, the values of the primal and dual residuals, described in Eq. (55) and (56), during the iterative process with different step size ρ are depicted in Fig. 18. It can be found that the primal and dual residuals converge within around 40 iterations, and a larger step size would result in fewer iterations. Nonetheless, the determination of the step size ρ is still an open issue for different problems. In this study, the values of ρ are chosen according to the methods suggested in [46] and previous research experience. To further demonstrate the superiority of the proposed distributed multi-energy DR methodology for the coordinated operation of buildings, the proposed distributed methodology as well as the centralized approach [13] were performed on a MES with the number of buildings ranging from 10 to 800. The comparative results

of the computational time for different number of buildings are given in Table 7. It can be observed that the runtime for both approaches increase with the growing number of buildings. Besides, the runtime of the proposed methodology increases approximately linearly with the increase of the number of buildings, while the runtime of the centralized approach grows more dramatically since it requires more time for the collection of all necessary information. Therefore, the proposed approach can be scalable to a large number of buildings as it converges in a suitable time.

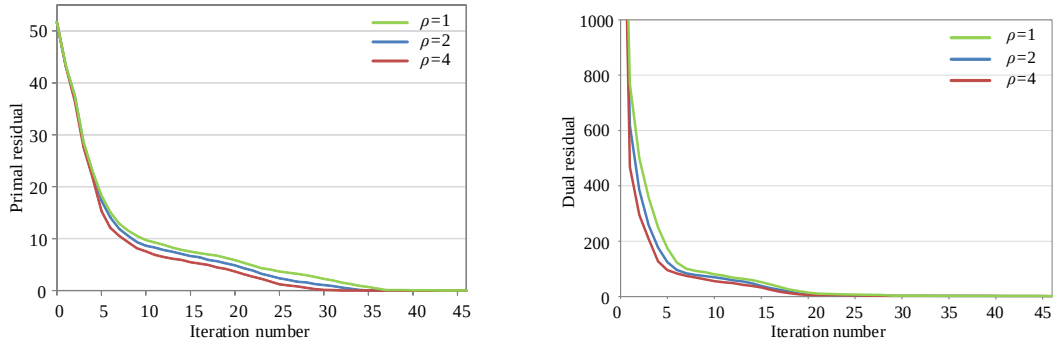

(a) (b)

Fig. 18 (a) Convergence process of primal residual, (b) Convergence process of dual residual.

Table 7 Comparisons of runtime for different approaches.

Number of buildings	Runtime (s)	
	Proposed approach	Centralized approach
10	48	76
20	92	158
50	221	345
100	416	512
200	824	1069
800	3215	10023

4.3.2 Advantages of the proposed distributed methodology

The proposed distributed multi-energy DR methodology has the following four advantages compared with centralized approaches.

- Privacy preservation: In the proposed distributed methodology, only the information associated with load demand and incentive signals are interacted between buildings and the aggregator, while the appliance-level information of all buildings is required to be transmitted to the aggregator to make DR decisions in centralized approaches. The proposed methodology can protect private information of users and thus is preferable.

- Light communication overhead: The distributed methodology can avoid communication congestion since the multi-energy DR problem is solved in a parallel fashion by individual buildings. In contrast, all decision variables of buildings will be transmitted in the communication networks for

centralized approaches, and the communication overhead would grow drastically with the increase of the number of buildings.

● Reliable communication: In the proposed hierarchical framework, buildings solve the local DR sub-problem independently. If there is a communication failure between a building and the aggregator, the remaining buildings can still provide their DR capabilities. Nevertheless, if the communication network between the aggregator and buildings is disconnected, the centralized DR approach is no longer available.

● High scalability: The results in Table 7 confirm that the distributed algorithm can converge in a more appropriate time than the centralized approach. Hence, the proposed distributed DR methodology is more scalable to incorporate a large number of buildings.

4.3.3 Comparison with related studies

Table 8 summarizes the DR methods in the recent literature. Various features including privacy, fairness, scalability are compared to show the novelties of the proposed distributed multi-energy DR methodology. Note that the customer comfort is not explicitly investigated, but the customer comfort is considered in the modeling of reducible appliances. Table 8 shows that no article involves the comprehensive features associated with the effectiveness and efficiency of the DR methods, and thus verifies the superiority of the proposed methodology.

Table 8 Summary of features of DR methods.

Reference	Privacy	Fairness	Scalability	Comfort	Detailed model	Optimality	CPU time	Multi-energy DR	Load prediction	Coordination	Approach
The proposed methodology	✓	✓	✓	✓	✓	✓	✓	✓	✓	✓	Distributed
[19]	✓		✓			✓	✓			✓	Distributed
[20]				✓		✓					Distributed
[21]				✓	✓	✓	✓				Distributed
[22]	✓				✓	✓			✓	✓	Distributed
[23]			✓			✓					Distributed
[24]	✓		✓		✓	✓	✓	✓			Distributed
[25]	✓				✓	✓		✓			Distributed
[47]	✓		✓	✓		✓	✓			✓	Distributed
[48]	✓		✓	✓	✓	✓	✓			✓	Distributed
[49]	✓		✓	✓		✓				✓	Distributed
[50]	✓	✓		✓		✓	✓			✓	Distributed
[51]	✓					✓			✓		Distributed

[52]	✓	✓				✓					Distributed
[53]	✓			✓		✓				✓	Distributed
[12]				✓	✓			✓	✓	✓	Centralized
[13]				✓	✓			✓			Centralized
[14]					✓	✓		✓			Centralized
[15]				✓		✓		✓	✓		Centralized
[16]				✓	✓			✓		✓	Centralized
[17]			✓	✓		✓	✓	✓			Centralized
[54]			✓			✓				✓	Centralized
[55]				✓	✓						Centralized
[56]						✓	✓		✓		Centralized

5 Conclusion

In this paper, a distributed multi-energy DR methodology is proposed to coordinate the optimal operation of heterogeneous smart buildings based on a hierarchical framework. A data-driven multi-energy demand prediction model using CapsNet is designed for the aggregator to simultaneously predict the multi-energy demands of building clusters. An exchange ADMM based distributed DR approach is then developed to iteratively solve the synergistic operation problem of buildings. The key findings from the simulation studies are summarized as follows: 1) The proposed methodology provides effective interactions between the aggregator and buildings and can achieve the optimal coordinated operation of building clusters to enhance the system operation performance. 2) The proposed methodology can incentivize buildings to fully exploit the load flexibility and multi-energy conversions to reduce their individual energy bills, and obtain the satisfactory overall economic and environmental efficiency. 3) The proposed distributed multi-energy DR methodology is more computationally efficient compared with the centralized method, especially for large-scale building clusters. Moreover, the proposed methodology guarantees the privacy preservation for buildings since only limited information needs to be exchanged between the aggregator and buildings.

Acknowledgment

This work was jointly supported by the Research Grants Council of the HKSAR Government (Grant No. R5020-18), the Innovation and Technology Commission of the HKSAR Government to the Hong Kong Branch of National Rail Transit Electrification and Automation Engineering Technology Research Center (Grant No. K-BBY1), the National Natural Science Foundation of China under Grant (51877072) and the Hunan Natural Science Foundation of China under Grant (2021JJ10019).

Appendix A. Mathematical formulation of multi-energy demand prediction

At time *t*, the matrix $\boldsymbol{y}_t \in R^{N\times L}$ is defined to indicate the multi-energy loads and weather data at *t* and $\boldsymbol{y}_{b,t}$ indicates the data of building *b*, as shown in Eq. (A.1). The loads at future time *t*+*t'* can be predicted based on the previous collected data as shown in Eq. (A.2), where $\hat{\boldsymbol{L}}_{t+t'}$ and $\hat{\boldsymbol{L}}_{b,t+t'}$ represents the predicted loads of all buildings and the predicted loads of building *b*, respectively; $\boldsymbol{\theta}$ represents the parameter set of the prediction model; *f* indicates the mapping function of the input and output of the model. The convolution computation is expressed by Eq. (A.3), where $\boldsymbol{\beta}_{tp}$, $\boldsymbol{b}_p$ and $\boldsymbol{x}_{tp}$ denote the convolution kernels, the bias and the *p*th feature map, respectively; $\otimes$ represents the convolution operator. The feature maps are then passed through the activation function $g(\cdot)$ to form a feature set $\boldsymbol{\sigma}_t = \{\sigma_{t|1}, \sigma_{t|2}, \cdots\}_t$ as shown in Eq. (A.4).

$$\boldsymbol{y}_t = \begin{bmatrix} \boldsymbol{y}_{1,t} & \boldsymbol{y}_{2,t} & \cdots & \boldsymbol{y}_{N,t} \end{bmatrix}^\top = \begin{bmatrix} y(1,1)_t & y(1,2)_t & \cdots & y(1,L)_t \\ y(2,1)_t & y(2,2)_t & \cdots & y(2,L)_t \\ \vdots & \vdots & & \vdots \\ y(N,1)_t & y(N,2)_t & \cdots & y(N,L)_t \end{bmatrix} \in R^{N\times L} \tag{A.1}$$

$$\hat{\boldsymbol{L}}_{t+t'} = \begin{bmatrix} \hat{\boldsymbol{L}}_{1,\ t+t'} & \hat{\boldsymbol{L}}_{2,\ t+t'} & \cdots & \hat{\boldsymbol{L}}_{N,\ t+t'} \end{bmatrix}^\top = f(\boldsymbol{y}_{t-\tau+1}, \boldsymbol{y}_{t-\tau+2}, \cdots, \boldsymbol{y}_t \,|\, \boldsymbol{\theta}) \tag{A.2}$$

$$\boldsymbol{y}_{tp} = g(\boldsymbol{y}_t \otimes \boldsymbol{\beta}_{tp} + \boldsymbol{b}_p) \tag{A.3}$$

$$\boldsymbol{\sigma}_t = g(\boldsymbol{w}\boldsymbol{y}_{tq} + \boldsymbol{b}) \tag{A.4}$$

Based on the above derivation, the multi-energy load prediction problem can be further represented as

$$\hat{\boldsymbol{L}}_{t+t'} = f'(\boldsymbol{\sigma}_{t-\tau+1}, \boldsymbol{\sigma}_{t-\tau+2}, \cdots, \boldsymbol{\sigma}_t \,|\, \boldsymbol{\theta}') \tag{A.5}$$

where f' denotes the mapping function of temporal dependency extraction, and $\boldsymbol{\theta}'$ represents the parameter set of capsule sub-network. The extracted spatial, coupling and weather features of multi-energy loads are chronologically encoded as primary capsules (P-Caps). Subsequently, the temporal dependencies among the extracted features are captured through the time capsule (T-Caps) layer by the dynamic routing mechanism, as follows,

$$\hat{\boldsymbol{\mu}}_{j|i} = \boldsymbol{W}_{ij}\boldsymbol{\mu}_i \tag{A.6}$$

$$c_{ij} = \frac{\exp(b_{ij})}{\sum_j \exp(b_{ij})} \tag{A.7}$$

$$\boldsymbol{s}_j = \sum_j c_{ij}\hat{\boldsymbol{\mu}}_{j|i} \tag{A.8}$$

$$\boldsymbol{v}_j = \frac{\left\|\boldsymbol{s}_j\right\|^2}{1+\left\|\boldsymbol{s}_j\right\|^2}\frac{\boldsymbol{s}_j}{\left\|\boldsymbol{s}_j\right\|} \tag{A.9}$$

$$b_{ij} = b_{ij} + \boldsymbol{v}_j \cdot \hat{\boldsymbol{\mu}}_{j|i} \tag{A.10}$$

where $\boldsymbol{\mu}_i$, $\hat{\boldsymbol{\mu}}_{j|i}$ and $\boldsymbol{W}_{ij}$ represent the features encapsulated in P-Caps i, the predicted temporal features for T-Caps j from P-Caps i, and the network weight matrix, respectively; c_{ij} denotes the coupling coefficient between P-Caps i and T-Caps j, and b_{ij} represents a temporary variable; $\boldsymbol{s}_j$ and $\boldsymbol{v}_j$ represent the input and output of T-Caps j, respectively. The P-Caps routes its prediction to the T-Caps by adjusting c_{ij} using the Softmax function (A.7). The input vector $\boldsymbol{s}_j$, which is the weighted sum of all predictions from the P-Caps layer, can be calculated by Eq. (A.8), and the output vector $\boldsymbol{v}_j$ is calculated by the Squashing function (A.9). The similarity between $\boldsymbol{v}_j$ and $\hat{\boldsymbol{\mu}}_{j|i}$ is determined by the dot product $\boldsymbol{v_j} \cdot \hat{\boldsymbol{\mu}}_{j|i}$. Specifically, if the predictions of temporal features from the P-Caps are similar with the output of T-Caps, $\boldsymbol{v_j} \cdot \hat{\boldsymbol{\mu}}_{j|i}$ will possess a big internal product thereby increasing the coupling coefficient c_{ij} by using Eqs. (A.10) and Eq. (A.6). Through the process of dynamically adjusting of the coupling coefficient c_{ij}, the temporal dependencies among the extracted spatial, coupling and weather features of multi-energy loads are captured in T-Caps.

The back-propagation algorithm is adopted to minimize the errors between the actual load data $\boldsymbol{L}_{t+t'}$ and the predicted results $\hat{\boldsymbol{L}}_{t+t'}$, and the loss function J is defined as,

$$J = \frac{1}{N \times L}\frac{1}{|\boldsymbol{T}|}\sum_{t\in\boldsymbol{T}}\left\|\boldsymbol{L}_{t+t'} - \hat{\boldsymbol{L}}_{t+t'}\right\|_F \tag{A.11}$$

where $\|\cdot\|_F$ and $|\boldsymbol{T}|$ denotes the Frobenius norm and the size of training samples, respectively. The network parameters including the weights $\boldsymbol{w}_l$ and the bias $\boldsymbol{b}_l$ are adjusted by the Adam algorithm [47], as follows,

$$\boldsymbol{w}_l = \boldsymbol{w}_{l-1} - \alpha_l \boldsymbol{m}_l / (\sqrt{\boldsymbol{e}_l} + \delta) \tag{A.12}$$

$$\boldsymbol{b}_l = \boldsymbol{b}_{l-1} - \alpha_l \boldsymbol{m}_l / (\sqrt{\boldsymbol{e}_l} + \delta) \tag{A.13}$$

$$\boldsymbol{m}_l = \varsigma_1 \boldsymbol{m}_{l-1} + (1-\varsigma_1)\cdot \partial J_l / \partial \boldsymbol{w}_l \tag{A.14}$$

$$\boldsymbol{e}_l = \varsigma_2 \boldsymbol{e}_{l-1} + (1-\varsigma_2)\cdot (\partial J_l / \partial \boldsymbol{w}_l)^2 \tag{A.15}$$

where $\boldsymbol{m}_l$ and $\boldsymbol{e}_l$ denote the first-order and second-order moment estimation vectors; ς_1 and ς_2 indicate exponential decay rate parameters; α_l denotes the learning rate. The training process is repeated until the training epoch l reaches the prescribed value.

Appendix B. Mathematical derivation of distributed multi-energy DR approach

It can be observed that the global energy equilibrium constraints Eq. (2) and Eq. (3) bridge the optimization problems for the aggregator and buildings. Suppose $-P_{M,t}=P_{a,t}^{\text{grid}}$ and $-V_{M,t}=V_{a,t}^{\text{gas}}$, where $P_{M,t}$ and $V_{M,t}$ are two auxiliary variables, and then Eq. (2) and Eq. (3) can be reformulated as,

$$\sum_{b=1}^{N} P_{b,t} + P_{M,t} = 0 \tag{B.1}$$

$$\sum_{b=1}^{N} V_{b,t} + V_{M,t} = 0 \tag{B.2}$$

Thereby, the original optimization problems can be reformulated as follows,

$$M = N + 1 \tag{B.3}$$

$$\min \sum_{b=1}^{N}\sum_{t=t_0}^{t_0+T} f_b(P_{b,t}) + \sum_{t=t_0}^{t_0+T} f_a(-P_{M,t}) + \sum_{b=1}^{N}\sum_{t=t_0}^{t_0+T} f_b(V_{b,t}) + \sum_{t=t_0}^{t_0+T} f_a(-V_{M,t}) \tag{B.4}$$

$$\text{s.t.} \quad \text{Eqs. (4)-(5), Eqs. (7)-(27), (29)} \tag{B.5}$$

$$\sum_{i=1}^{M} P_{i,t} = 0,\ t \in \{t_0, ..., t_0+T\} \tag{B.6}$$

$$\sum_{i=1}^{M} V_{i,t} = 0,\ t \in \{t_0, ..., t_0+T\} \tag{B.7}$$

where M denotes the total number of the aggregator and buildings. The equilibrium constraints (B.6)-(B.7) force that the multi-energy demand and supply of all participants are balanced in each time slot. To determine the optimal multi-energy DR approach, a distributed optimization algorithm based on the exchange ADMM is developed. For notational convenience, $\boldsymbol{x}$ represents the decision variables for the optimization problem Eqs. (B.4)-(B.7), and λ_t, y_t represent the dual variables associated with Eqs. (B.6)-(B.7). According to the unscaled form of the exchange ADMM in [46], the problem Eq. (B.4) can be decomposed into decision-making sub-problems with an iterative process, as follows,

$$\begin{aligned}\min_{\boldsymbol{x}} \sum_{i=1}^{M}\sum_{t=t_0}^{t_0+T} \big(& f_i(P_{i,t}) + f_i(V_{i,t}) + \lambda_t^{\,k} \cdot P_{i,t} + y_t^{\,k} \cdot V_{i,t} \\ & + \frac{\rho}{2}\left\| P_{i,t} - (P_{i,t}^{\,k} - \overline{P}_t^{\,k}) \right\|_2^2 + \frac{\rho}{2}\left\| V_{i,t} - (V_{i,t}^{\,k} - \overline{V}_t^{\,k}) \right\|_2^2 \big)\end{aligned} \tag{B.8}$$

$$\text{s.t.} \quad \text{Eq. (B.5)} \tag{B.9}$$

The dual variables are updated as,

$$\lambda_t^{\,k+1} = \lambda_t^{\,k} + \rho \overline{P}_t^{\,k+1} \tag{B.10}$$

$$y_t^{\,k+1} = y_t^{\,k} + \rho \overline{V}_t^{\,k+1} \tag{B.11}$$

where k is the index of the iteration; $\bar{P}_t^k = (1/M)\sum_{i=1}^{M} P_{i.t}^k, \bar{V}_t^k = (1/M)\sum_{i=1}^{M} V_{i.t}^k$ represent the average power and natural gas of all participants, respectively; $\rho > 0$ denotes the penalty parameter and is used

as the step size for dual update. For mathematical conciseness, Eq. (B.8), (B.10)-(B.11) can be written in a scaled form as Eqs. (B.12)-(B.14), where λ_t and y_t are scaled with $u_t = \lambda_t/\rho$ and $\alpha_t = y_t/\rho$, respectively.

$$\min_{\boldsymbol{x}} \sum_{i=1}^{M} \sum_{t=t_0}^{t_0+T} \left(f_i(P_{i,t}) + f_i(V_{i,t}) + \frac{\rho}{2} \left\| P_{i,t} - P_{i,t}{}^k + \overline{P}_t^k + u_t^k \right\|_2^2 + \frac{\rho}{2} \left\| V_{i,t} - V_{i,t}{}^k + \overline{V}_t^k + \alpha_t^k \right\|_2^2 \right) \tag{B.12}$$

$$u_t{}^{k+1} = u_t{}^k + \overline{P}_t^{k+1} \tag{B.13}$$

$$\alpha_t{}^{k+1} = \alpha_t{}^k + \overline{V}_t^{k+1} \tag{B.14}$$

The local sub-problem for each building at the *k*th iteration is formulated as follows,

$$\min_{\boldsymbol{x} \setminus P_{M,t}, V_{M,t}} \sum_{t=t_0}^{t_0+T} \left(f_b(P_{b,t}) + f_b(V_{b,t}) + \frac{\rho}{2} \left\| P_{b,t} - P_{b,t}{}^k + \overline{P}_t^k + u_t^k \right\|_2^2 + \frac{\rho}{2} \left\| V_{b,t} - V_{b,t}{}^k + \overline{V}_t^k + \alpha_t^k \right\|_2^2 \right) \tag{B.15}$$

$$\text{s.t.} \quad \text{Eqs. (7)-(27), (29)} \tag{B.16}$$

For the aggregator, the local optimization sub-problem can be expressed as,

$$\min_{P_{M,t}, V_{M,t}} \sum_{t=t_0}^{t_0+T} \left(f_a(-P_{M,t}) + f_a(-V_{M,t}) + \frac{\rho}{2} \left\| P_{M,t} - P_{M,t}{}^k + \overline{P}_t^k + u_t^k \right\|_2^2 + \frac{\rho}{2} \left\| V_{M,t} - V_{M,t}{}^k + \overline{V}_t^k + \alpha_t^k \right\|_2^2 \right) \tag{B.17}$$

$$\text{s.t.} \quad \text{Eqs. (4)-(5)} \tag{B.18}$$

In each iteration *k*, the aggregator and buildings update their solutions according to Eqs. (B.15)-(B.18), and the average power and natural gas of all participants $\overline{P}_t^k$ and $\overline{V}_t^k$ are correspondingly updated. For the next iteration *k*+1, the aggregator send the updated incentive signals u_t and α_t to the buildings based on Eqs. (B.13)-(B.14), and the buildings solve their individual sub-problems according to the incentive signals and then send back their energy demand information. The convergence criteria for the distributed iterative optimization are given by the primal residuals $r_{P,t}^k$, $r_{V,t}^k$ and dual residuals $s_{i,P,t}^k$, $s_{i,V,t}^k$ [46],

$$r_{P,t}^k = \overline{P}_t^k \tag{B.19}$$

$$r_{V,t}^k = \overline{V}_t^k \tag{B.20}$$

$$s_{i,P,t}^k = -\rho[P_{i,t}^k - P_{i,t}^{k-1} + (\overline{P}_t^{k-1} - \overline{P}_t^k)] \tag{B.21}$$

$$s_{i,V,t}^k = -\rho[V_{i,t}^k - V_{i,t}^{k-1} + (\overline{V}_t^{k-1} - \overline{V}_t^k)] \tag{B.22}$$

The stopping criteria are as follows,

$$\left\| r_{P,t}^k \right\|_2 + \left\| r_{V,t}^k \right\|_2 \le \varepsilon^{\text{pri}}, t \in \{t_0, ..., t_0+T\} \tag{B.23}$$

$$\left\| s_{i,P,t}^k \right\|_2 + \left\| s_{i,V,t}^k \right\|_2 \le \varepsilon^{\text{dual}}, i = 1, ..., M, t \in \{t_0, ..., t_0+T\} \tag{B.24}$$

where ε^{pri} ($\varepsilon^{\text{pri}} > 0$) and $\varepsilon^{\text{dual}}$ ($\varepsilon^{\text{dual}} > 0$) are primary and dual feasibility tolerances.

References

[1] Afzalan M, Jazizadeh F. Residential loads flexibility potential for demand response using energy consumption patterns and user segments. Appl Energy 2019; 254: 113693.

[2] Wang J, Zhong H, Ma Z, Xia Q, Kang C. Review and prospect of integrated demand response in the multi-energy system. Appl Energy 2017; 202: 772-782.

[3] Dadashi-Rad M H, Ghasemi-Marzbali A, Ahangar R A. Modeling and planning of smart buildings energy in power system considering demand response. Energy 2020; 213: 118770.

[4] Tang R, Wang S. Model predictive control for thermal energy storage and thermal comfort optimization of building demand response in smart grids. Appl Energy 2019; 242: 873-882.

[5] Huang W, Zhang N, Kang C, Li M, Huo M. From demand response to integrated demand response: review and prospect of research and application. Prot Control Mod Power Syst 2019; 4(1): 1-13.

[6] Muratori M, Rizzoni G. Residential demand response: Dynamic energy management and time-varying electricity pricing. IEEE Trans Power Syst 2016; 31(2): 1108-1117.

[7] Paterakis N G, Erdinç O, Pappi I N, Bakirtzis A G, Catalão J P S. Coordinated operation of a neighborhood of smart households comprising electric vehicles, energy storage and distributed generation. IEEE Trans Smart Grid 2016; 7(6): 2736-2747.

[8] Wang Z, Crawley J, Li F G N, Lowe R. Sizing of district heating systems based on smart meter data: Quantifying the aggregated domestic energy demand and demand diversity in the UK. Energy 2020; 193: 1331-1342.

[9] Zhou B, Cao Y, Li C, Wu Q, Liu N, Huang S, et al. Many-criteria optimality of coordinated demand response with heterogeneous households. Energy 2020; 207: 118267.

[10] Xie G, Chen X, Weng Y. An integrated Gaussian process modeling framework for residential load prediction. IEEE Trans Power Syst 2018; 33(6):7238-7248.

[11] Tan Z, De G, Li M, Lin H, Yang S, Huang L, et al. Combined electricity-heat-cooling-gas load forecasting model for integrated energy system based on multi-task learning and least square support vector machine. J Clean Prod 2020; 248: 119252.

[12] Niu J, Tian Z, Zhu J, Yue L. Implementation of a price-driven demand response in a distributed energy system with multi-energy flexibility measures. Energy Conv Manag 2020; 208: 112575.

[13] Çiçek A, Şengör İ, Erenoğlu A K, Erdinç O. Decision making mechanism for a smart neighborhood fed by multi-energy systems considering demand response. Energy 2020; 208: 118323.

[14] Salehi J, Namvar A, Gazijahani F S. Scenario-based Co-Optimization of neighboring multi carrier smart buildings under demand response exchange. J Clean Prod 2019; 235: 1483-1498.

[15] Wang Y, Ma Y, Song F, Ma Y, Qi C, Huang F, et al. Economic and efficient multi-objective operation optimization of integrated energy system considering electro-thermal demand response. Energy 2020; 205: 118022.

[16] Wang D, Hu Q, Jia H, Hou K, Du W, Chen N, et al. Integrated demand response in district electricity-heating network considering double auction retail energy market based on demand-side energy stations. Appl Energy 2019; 248: 656-678.

[17] Shao C, Ding Y, Siano P, Lin Z. A framework for incorporating demand response of smart buildings into the integrated heat and electricity energy system. IEEE Trans Ind Electron 2019; 66(2): 1465-1475.

[18] Liu G, Jiang T, Ollis T B, Zhang X, Tomsovic K. Distributed energy management for community microgrids considering network operational constraints and building thermal dynamics. Appl Energy 2019; 239: 83-95.

[19] McNamara P, McLoone S. Hierarchical demand response for peak minimization using Dantzig-Wolfe decomposition. IEEE Trans Smart Grid 2015; 6(6): 2807-2815.

[20] Jia L, Tong L. Dynamic pricing and distributed energy management for demand response. An MILP-based optimal power flow in multicarrier energy systems. IEEE Trans Smart Grid 2016; 7(2): 1128-1136.
[21] Latifi M, Rastegarnia A, Khalili A, Vahidpour V, Sanei S. A distributed game-theoretic demand response with multi-class appliance control in smart grid. Electr Power Syst Res 2019; 176: 105946.
[22] Cai H, You S, Wu J. Agent-based distributed demand response in district heating systems. Appl Energy 2020; 262: 114403.
[23] Ruan G, Zhong H, Wang J, Xia Q, Kang C. Neural-network-based Lagrange multiplier selection for distributed demand response in smart grid. Appl Energy 2020; 264: 114636.
[24] Bahrami S, Toulabi M, Ranjbar S, Moeini-Aghtaie M, Ranjbar A M. A decentralized energy management framework for energy hubs in dynamic pricing markets. IEEE Trans Smart Grid 2018; 9(6): 6780-6792.
[25] Zhong W, Xie K, Liu Y, Yang C, Xie S, Zhang Y. Distributed Demand Response for Multienergy Residential Communities With Incomplete Information. IEEE Trans Ind Inform 2021; 17(1): 547-557.
[26] Zhou B, Meng Y, Huang W, Wang H, Deng L, Huang S, et al. Multi-energy net load forecasting for integrated local energy systems with heterogeneous prosumers. Int J Electr Power Energy Syst 2021; 126: 106542.
[27] Wang S, Wang S, Chen H, Gu Q. Multi-energy load forecasting for regional integrated energy systems considering temporal dynamic and coupling characteristics. Energy 2020; 195: 116964.
[28] Zhang L, Shi J, Wang L, Xu C. Electricity, heat, and gas load forecasting based on deep multitask learning in industrial-park integrated energy system. Entropy 2020; 22(12): 1355.
[29] Xie G, Chen X, Weng Y. An integrated Gaussian process modeling framework for residential load prediction. IEEE Trans Power Syst 2018; 33(6): 7238-7248.
[30] Wang X, Wang S, Zhao Q, Wang S, Fu L. A multi-energy load prediction model based on deep multi-task learning and ensemble approach for regional integrated energy systems. Int J Electr Power Energy Syst 2021; 126: 106583.
[31] Yildiz B, Bilbao J I, Sproul A B. A review and analysis of regression and machine learning models on commercial building electricity load forecasting. Renew Sust Energ Rev 2017; 73: 1104-1122.
[32] Sabour S, Frosst N, Hinton G E. Dynamic routing between capsules. in Proc 31st Int Conf Neural Inf Process Syst 2017.
[33] Peng D, Zhang D, Liu C, Lu J. BG-SAC: entity relationship classification model based on self-attention supported capsule networks. Appl Soft Comput 2020; 91: 106186.
[34] Zhang K, Zhou B, Or S W, Li C, Chung C Y, Voropai N. Optimal coordinated control of multi-renewable-to-hydrogen production system for hydrogen fueling stations. IEEE Trans Ind Appl 2021; DOI: 10.1109/TIA.2021.3093841.
[35] Lv C, Yu H, Li P, Wang C, Xu X, Li S, et al. Model predictive control based robust scheduling of community integrated energy system with operational flexibility. Appl Energy 2019; 243: 250-265.
[36] Erdinç O, Taşcıkaraoğlu A, Paterakis N G, Eren Y, Catalão J P S. End-user comfort oriented day-ahead planning for responsive residential HVAC demand aggregation considering weather forecasts. IEEE Trans Smart Grid 2017; 8(1): 362-372.
[37] Joo I Y, Choi D H. Optimal household appliance scheduling considering consumer's electricity bill target. IEEE Trans Consum Electron 2017; 63(1): 19-27.
[38] Chu W C, Chen Y P, Xu Z W, Lee W J. Multiregion short-term load forecasting in consideration of HI and load/weather diversity. IEEE Trans Ind Appl 2011; 47(1): 232-237.
[39] Wang H, Meng K, Luo F, Dong Z, Verbic G, Xu Z, et al. Demand response through smart home energy management using thermal inertia. in Proc Aust Univ Power Eng Conf 2013; 1-6.
[40] Shao C, Wang X, Shahidehpour M, Wang X, Wang B. An MILP-based optimal power flow in multicarrier energy systems. IEEE Trans Sustain Energy 2017; 8(1): 239-248.

[41] Wang Y, Wang Y, Huang Y, Li F, Zeng M, Li J, et al. Planning and operation method of the regional integrated energy system considering economy and environment. Energy 2019; 171: 731-750.
[42] Elsied M, Oukaour A, Gualous H, Lo Brutto O A. Optimal economic and environment operation of micro-grid power systems. Energy Conv Manag 2016; 122: 182-194.
[43] Guo Y, Xiong J, Xu S, Su W. Two-stage economic operation of microgrid-like electric vehicle parking deck. IEEE Trans Smart Grid 2016; 7(3): 1703-1712.
[44] Rezaee S, Farjah E, Khorramdel B. Probabilistic analysis of plug-in electric vehicles impact on electrical grid through homes and parking lots. IEEE Trans Sustain Energy 2013; 4(4): 1024-1033.
[45] Diekerhof M, Peterssen F, Monti A. Hierarchical distributed robust optimization for demand response services. IEEE Trans Smart Grid 2018; 9(6): 6018-6029.
[46] Boyd S, Parikh N, Chu E, Peleato B, Eckstein J. Distributed optimization and statistical learning via the alternating direction method of multipliers. Found Trendsin Mach Learn 2011; 3(1): 1-122.
[47] de Souza Dutra M D, Alguacil N. Optimal residential users coordination via demand response: an exact distributed framework. Appl Energy 2020; 279: 115851.
[48] Mhanna S, Chapman A C, Verbič G. A fast distributed algorithm for large-scale demand response aggregation. IEEE Trans Smart Grid 2016; 7(4): 2094-2107.
[49] Safdarian A, Fotuhi-Firuzabad M, Lehtonen M. Optimal residential load management in smart grids: a decentralized framework. IEEE Trans Smart Grid 2016; 7(4): 1836-1845.
[50] Fan S, Ai Q, Piao L. Bargaining-based cooperative energy trading for distribution company and demand response. Appl Energy 2018; 226: 469-482.
[51] Tan Z, Yang P, Nehorai A. An optimal and distributed demand response strategy with electric vehicles in the smart grid. IEEE Trans Smart Grid 2014; 5(2): 861-869.
[52] Baharlouei Z, Hashemi M. Efficiency-fairness trade-off in privacy-preserving autonomous demand side management. IEEE Trans Smart Grid 2014; 5(2): 799-808.
[53] Yu M, Hong S H. Incentive-based demand response considering hierarchical electricity market: a stackelberg game approach. Appl Energy 2017; 203: 267-279.
[54] Yu M, Hong S H. Supply–demand balancing for power management in smart grid: a stackelberg game approach. Appl Energy 2016; 164: 702-710.
[55] de Souza Dutra MD, Anjos MF, Le Digabel S. A realistic energy optimization model for smart-home appliances. Int J Energy Res 2018; 43(8):3237-62.
[56] Rashidizadeh-Kermani H, Vahedipour-Dahraie M, Shafie-khah M, Catalão JPS. Stochastic programming model for scheduling demand response aggregators considering uncertain market prices and demands. Int J Electr Power Energy Syst 2019; 113:528-38.
[57] Kingma D P, Ba J. Adam: A method for stochastic optimization. arXiv preprint arXiv:1412.6980, 2014.